Modular treatment of arsenic-laden brackish groundwater using solar-powered subsurface arsenic removal (SAR) and membrane capacitive deionization (MCDI) in Vietnam

U. Hellriegel, E. E. Cañas Kurz, T. V. Luong, J. Bundschuh and J. Hoinkis

ABSTRACT

To evaluate energy efficient concepts for the modular treatment of brackish water, pilot trials for groundwater desalination and arsenic (As) removal were carried out in the Mekong Delta, Vietnam. Groundwater here is affected by naturally occurring high iron (Fe^{2+}) and As concentrations, while, in coastal regions, groundwater is additionally contaminated by high salinity mostly due to seawater intrusion. Desalination was conducted by membrane capacitive deionization (MCDI), which shows low specific energy consumption (SEC). Anoxic groundwater with As(III) and Fe^{2+} was treated using a pre-oxidation step called subsurface arsenic removal (SAR) with the main advantage that no As-laden waste is produced. The pilot plant was operated using a photovoltaic system (3 kW_p) and a small wind turbine (2 kW_p). The SEC of drinking water produced was 3.97 kWh/m^3. Total dissolved solids (TDS) of 1,560 mg/L were lowered to 188 mg/L, while Fe^{2+} was reduced from 1.8 mg/L to the below detection limit and As from 2.3 to 0.18 μg/L. The results show that SAR is a feasible remediation technique for Fe^{2+} and As removal in remote areas, and demonstrate the potential of MCDI for brackish water desalination coupled with renewable energies. However, improvements in energy demand of the MCDI module can still be achieved.

Key words | arsenic removal, coastal groundwater, desalination, MCDI, pilot scale, renewable energy

HIGHLIGHTS

- Pilot trials for groundwater treatment were successfully carried out in the Mekong Delta, Vietnam.
- Subsurface arsenic (SAR) and iron removal and membrane capacitive deionization (MCDI) achieved drinking water standard.
- The process was run by renewable energy (photovoltaic and wind turbine).
- Efficiency improvements in energy conversion losses are needed for the MCDI.
- The findings can serve as an example for coastal groundwater treatment.

U. Hellriegel
E. E. Cañas Kurz
J. Hoinkis (corresponding author)
Center of Applied Research,
Karlsruhe University of Applied Sciences,
Moltkestr. 30, 76133 Karlsruhe,
Germany
E-mail: *jan.hoinkis@hs-karlsruhe.de*

U. Hellriegel
E. E. Cañas Kurz
Department of Chemistry and Chemical Technologies,
University of Calabria,
Via Pietro Bucci 12/C, 87036 Arcavacata di Rende, Cosenza,
Italy
and
Institute on Membrane Technology,
National Research Council (ITM-CNR),
Via Pietro Bucci 17/C, 87036 Arcavacata di Rende, Cosenza,
Italy

T. V. Luong
Department of Mechatronics and Sensor Systems Technology,
Vietnamese-German University,
Le Lai Street, 822096 Binh Duong Province,
Vietnam
and
Department of Separation Science, School of Engineering Science,
Lappeenranta-Lahti University of Technology,
Sammonkatu 12, 50130 Mikkeli,
Finland

J. Bundschuh
J. Hoinkis
Faculty of Health, Engineering and Sciences,
University of Southern Queensland,
West Street, Toowoomba, 4350 Queensland,
Australia

J. Bundschuh
UNESCO Chair on Groundwater Arsenic Within the 2030 Agenda for Sustainable Development,
School of Civil Engineering and Surveying,
University of Southern Queensland,
4350 Queensland,
Australia

doi: 10.2166/wrd.2020.031

GRAPHICAL ABSTRACT

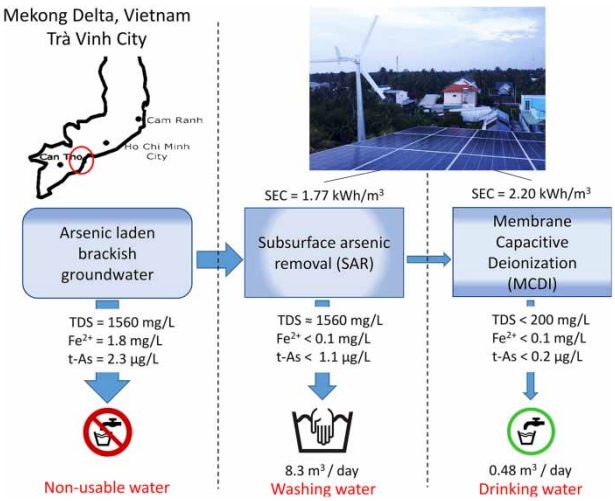

INTRODUCTION

Currently, about 600 million people worldwide live in low-elevation coastal zones affected by progressive salinization (Wheeler 2011; Dasgupta *et al.* 2014a). Groundwater in coastal line aquifers is often affected by seawater intrusion due to overextraction and rising sea levels, which will be aggravated by climate change in the future. The salinity level is subject to seasonal variations during dry and wet periods, and tidal channels are an important potential source of high salinity water (Brecht *et al.* 2012; Dasgupta *et al.* 2014b; Colombani *et al.* 2016). In the Mekong Delta, the salt concentration in the groundwater varies between 1 and >10 g/L (Wassmann *et al.* 2004; Hien *et al.* 2009; Ngo-Duc 2014; Vu *et al.* 2018).

In addition, high arsenic (As) concentrations are widespread in the groundwater of tidal delta plains in South and Southeast Asia such as the Ganges–Brahmaputra–Meghna in Bangladesh, the Irrawaddy delta in Myanmar, and the Mekong and Red river delta in Vietnam (Smedley *et al.* 2002; Buschmann *et al.* 2008; Winkel *et al.* 2011; Ayers *et al.* 2016; Wang *et al.* 2018; Le Luu 2019). As dissolved in groundwater in South Asia is caused by subsurface sediments, where As is adsorbed onto hydrous ferric oxides (HFOs; Hossain *et al.* 2012; Sankar *et al.* 2014; Wang *et al.* 2018). Manganese is also often co-associated with iron. Previous studies confirmed that reductive dissolution of HFOs driven by microbial metabolism of organic matter results in increased concentrations of dissolved As in shallow groundwater in Bangladesh (Nickson *et al.* 2000) and other South Asian countries (Berg *et al.* 2001; Datta *et al.* 2014; Stopelli *et al.* 2020).

Goal and scope

This study was carried out within the German joint research project *WaKap* as part of one of three plants installed around the Mekong Delta for subsurface arsenic removal (SAR) and/or desalination of brackish water (WaKap 2016). This study focused on the implementation of a combined desalination and As remediation technology using membrane capacitive deionization (MCDI) and SAR, respectively.

Combining the two technologies aimed at a robust, sustainable and easy-to-use approach for high removal and water recovery efficiencies as well as low energy demand. Additionally, an important goal was to evaluate the supply of the system with renewable power sources such as solar (photovoltaic, PV) and wind (wind turbine, WT) power. A sustainability assessment and evaluation of the system was

carried out taking environmental and socio-economic aspects of the region into consideration (WaKap 2016; Fritz *et al.* 2020).

State of the art

Capacitive deionization (CDI) is a relatively new electrochemical desalination process with the general advantage of low specific energy consumption (SEC) since no high pressure pumps or heat sources are required. In this process, saline water flows between two porous electrodes made of activated carbon, on which a voltage is applied. The positive ions are thereby attracted to the negatively charged electrode and vice versa. After the electrodes are loaded, the salt ions can be removed by reversing the polarity of the electrodes. Through a constant change of charge (desalination) and discharge (regeneration), two water streams with desalinated water or concentrated salt water are produced (AlMarzooqi *et al.* 2014; Wang *et al.* 2019). Mounting ion exchange membranes in front of the electrodes enhances the desalination performance of the CDI module, because co-ion leakage is lowered and the discharge phase can be shortened (Zhao *et al.* 2013). This technology is then defined as MCDI. CDI is ideally suited for decentralized applications since it can be directly powered by solar PV energy (Tan *et al.* 2018).

SAR aims at the removal of As, Fe and Mn, in advance of the MCDI process. For this, part of the extracted groundwater is enriched with oxygen and introduced back into the underground (aquifer). Dissolved iron (Fe^{2+}) and manganese (Mn^{2+}) ions are oxidized and precipitated as sparingly soluble (hydr)oxides forming a zone with treated water around the re-injection zone in the aquifer that is free of dissolved Fe^{2+} and Mn^{2+} (Sarkar & Rahman 2001; Sen Gupta 2008; van Halem 2011; Rahman *et al.* 2014; Kundu *et al.* 2018). Under anoxic conditions, as in South Asia, groundwater principally contains arsenite in the form of H_3AsO_3 which is oxidized through SAR to arsenate (depending on pH conditions to $H_2AsO_4^-$ or $HAsO_4^{2-}$) and is then immobilized in the soil by co-adsorption onto the iron and manganese(hydr)oxides (Rahman *et al.* 2015; Annaduzzaman *et al.* 2018; Luong *et al.* 2018). The salient advantage of the process is that no As-laden (waste)stream is produced, since As is immobilized in the aquifer, where it naturally occurs (Rott & Friedle 2000; van Halem *et al.* 2009; Stopelli *et al.* 2020).

In contrast, every membrane-based technology for removing As from water creates an As-concentrated volume as a co-product, and safe disposal methods need to be evaluated. Examples are reverse osmosis (RO) or nano-, ultra- and microfiltration (Shih 2005; Figoli *et al.* 2016). The RO and dense NF membranes can remove sufficient As to meet drinking water standards (Schmidt *et al.* 2016; Figoli *et al.* 2020). UF and MF treatments need a coagulation/flocculation process upfront to remove As, due to the membranes having a course porosity, which cannot retain dissolved As (Ćurko *et al.* 2011; Elcik *et al.* 2013).

Renewable energy systems, especially PV panels, are mostly needed on the numerous Vietnamese islands without stable grid connections. Due to a generous feed-in tariff of US$93.5/MWh for new projects, together with supporting policies such as tax exemptions, Vietnam experienced a solar PV installation boom, also on the main land in the first half of 2019, with installed capacity increasing to 4,450 MW (Do *et al.* 2020). Underlying drivers include the government's desire to enhance energy self-sufficiency and the public's demand for local environmental quality.

MATERIALS AND METHODS

Pilot plant

The modular pilot plant for the desalination of brackish water including the subsurface removal of Fe^{2+}, Mn^{2+} and As was installed in June 2018 on a household rooftop in Trà Vinh city, in a coastal region in the Mekong Delta, Vietnam. The process scheme of the system consisting of an MCDI (CapDI, Voltea®) plant with upfront SAR (*FERMA-NOX®-Wasseraufbereitung* type BV 104) for iron and As removal is shown in Figure 1. Two different product streams are produced from the modular system: As and Fe^{2+} free treated water from SAR is stored in T1 (e.g. for washing purposes), while drinking water from the MCDI is stored in T2.

(1) *SAR*: A submersible pump (PENTAX® 4ST 14-8) is used to pump the groundwater (water table at 2 m below the surface) through a sand filter (1354 FRP Vessel, sand

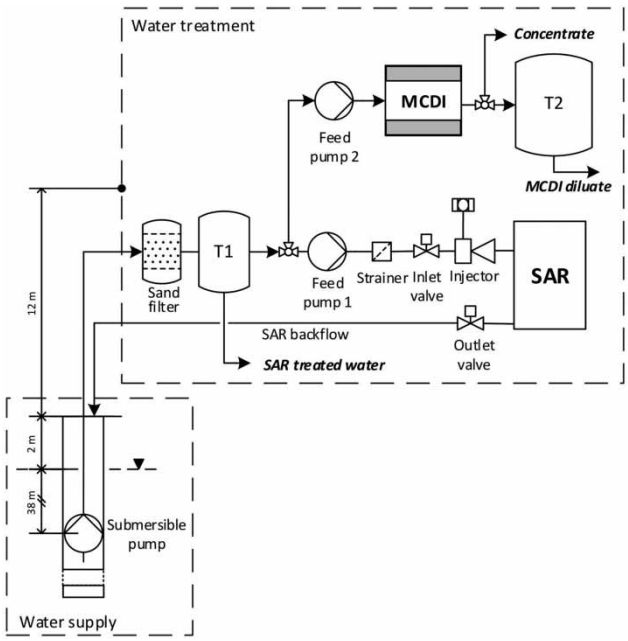

Figure 1 | Scheme of the modular pilot plant including *water supply* with submersible feed pump and *water treatment* consisting of SAR and MCDI with pre-filter (sand filter) and storage tanks T1 (SAR-treated water) and T2 (MCDI diluate).

0.5–1 mm as filtration media) to prevent particles from passing into a storage tank on the rooftop (T1, 12 m above the surface). The treatment process is divided into the aeration and infiltration cycles: firstly, water from T1 is aerated with an air injector using a booster pump (feed pump 1; GRUNDFOS® SCALA2) and stored in the SAR tank (900 L). Then, the oxygen-enriched water is infiltrated back into the aquifer by gravity (SAR backflow). Iron oxidation and As adsorption take place underground, and water with very low, nontoxic concentrations of As is obtained around the well. Subsequently, all extracted water from the well, which is stored in T1, can be used by the household or further treated with MCDI.

Aeration and infiltration cycles must be repeated constantly to maintain the oxygenated zone around the well. When water is extracted from the well, oxidation–adsorption takes place in the oxidation zone and the infiltrated oxygen is gradually consumed. In order to avoid leakage of As or any other contaminant, a daily water extraction limit V_E is calculated as a design parameter based on the previous experience of the manufacturer and fixed for using SAR (Luong *et al.* 2018, 2019; Cañas Kurz *et al.* 2020). With a daily operation of two infiltration cycles (each cycle $V_I = 900$ L), the maximum designed capacity of the SAR plant is $V_E = 8.3\ m^3/d$. This leads to an infiltration/extraction ratio at the pilot site of $Q_E = V_I/V_E = 0.22\ m^3/m^3$. Since the oxygenated water is always infiltrated back into the aquifer, another advantage of the process is that no water is lost and no waste stream is produced.

(2) *MCDI desalination*: Secondly, a home-made MCDI unit with a commercial electrode module (Voltea B.V® Model C3) is used for the desalination of the groundwater to obtain drinking water (see Figure 2). The information provided by the manufacturer is the total surface area of the electrodes at 3.7 m^2 as well as sulfonyl and quaternary ammonium groups as active functionality groups for the cation and anion exchange membranes, respectively. By using a diaphragm pump (feed pump 2; SHURflo® 8000-243-155), SAR-treated water from T1 is passed through the MCDI module in alternate cycles for desalination (charge) and regeneration of the electrodes (discharge). The MCDI module is operated with constant current (CC) during both phases with reversed voltage in the discharge phase using an XP power supply (XP Power HDS 1500 PS12, with a maximum electrical current at

Figure 2 | MCDI pilot plant for desalination including the electrode module (Voltea C3) and power supply (XP Power HDS 1500 PS12).

the outlet $I_{max} = 100$ A). To determine the TDS removal, the electrical conductivity (*EC*) of the water stream was measured at the inlet and the outlet of the MCDI module with conductivity sensors from Supmea (SPE-EC100). The *EC* in μS/cm was then converted to a TDS concentration in mg/L by multiplying the *EC* value with the factor $K = 0.5$ (Walton 1989). This factor was confirmed experimentally to fit to the concentrations used in these studies by comparing the *EC* values of solutions with known TDS concentrations up to 1.65 g/L. The diluate of the MCDI is stored in T2, which is connected to the water supply, whereas the concentrate effluent is discharged directly into the sewer.

The pilot plant is operated by renewable energy (see Figure 3). A 2 kW_p WT (Hummer, 2 kW-Windspot 220 V) is controlled by an on-grid inverter, and a 3 kW_p solar PV system (SUNERGY, SUN72M, monocrystalline) is connected with a hybrid inverter (Goodwee, GW-3648) that includes two lithium batteries (Scared sun, 2,400 Wh 50 Ah) for a total battery storage capacity of 4.8 kWh. The pilot plant is supplied directly by PV power. Excess energy is fed into the regional power grid; if energy is required, for example at night, the plant is powered additionally by the battery storage. If the battery state of charge (SOC) is lower than 20%, the plant can be supplied through the grid. A separate net-metering system controls the in-going and out-going energy of the latter. Additional power generation from the WT is directly fed into the grid.

Furthermore, a home-made weather station including anemometer (Davies, 6410) and pyranometer (Apogee Instr., SP-215) is used for monitoring wind direction, wind speed, ambient temperature and solar radiation at the pilot site.

Laboratory tests

Laboratory tests were carried out in order to compare the performance of two MCDI modules with different setups. The described MCDI module of the pilot plant-treating groundwater in Trà Vinh is hereinafter defined as setup 1. A second MCDI module consisting of the development kit (DK) of Voltea B.V.® (maximum electrical current at the outlet $I_{max} = 60$ A) using the same type of electrode module (C3 model) and the automation and control system is used to desalinate NaCl (>99.8%) diluted with deionized water ($EC = 3.29$ mS/cm) under laboratory conditions. The DK includes conductivity sensors at the inlet and outlet as well as a pressure sensor to constantly record the same parameters as the pilot plant. This installation is subsequently defined as setup 2.

The focus in evaluating the performance of each setup is its *SEC*, which is defined by the used energy divided by the produced volume of the diluate (V_d). Two different types are therefore defined. One SEC_{CDI} for desalinating the water in the MCDI module to separate the salt ions from the water, taking into account the electrical power input measured at the outlet of the according power supply (P_{CDI}) and (t),

Figure 3 | PV system and WT at the pilot plant location in Trà Vinh, Mekong Delta, Vietnam.

and another $SEC_{CDI,sys}$ for the system, which includes the performance of the diaphragm pump (P_p). They are calculated as stated in the following equations:

$$SEC_{CDI} = \frac{P_{CDI} \cdot t}{V_d} \quad (1)$$

$$SEC_{CDI,sys} = \frac{(P_{CDI} + P_p) \cdot t}{V_d} . \quad (2)$$

To compare the performance of the MCDI modules of desalinating water, the charge efficiency η_{ch} can be used. Hereby, the electrical current I_{ch} during charge time is compared to the amount of adsorbed ions in the electrodes as stated in the following equation:

$$\eta_{ch} = \frac{\Delta m / M}{Q / F} \quad (3)$$

where Δm is the removed amount of total dissolved solids (TDS) in g, M the molar mass, Q the electrical charge and F the Faraday constant. For all calculations, the molar mass of NaCl ($M = 58.5$ g/mol) is assumed.

Sample analysis

The raw water samples were taken directly from the pipe behind the submersible pump after water was extracted for some time. Subsequently, the samples were acidified for conservation as prescribed by the standard DIN EN ISO 5667–3.

Values for pH and *EC* were measured on site using a portable sensor (WTW Multi-Parameter 3430). Total Fe and Mn were measured with the flame technique using atomic adsorption spectrometry (AAS, Analytik Jena, contrAA® 300) and a 50 mm burner with an air/acetylene gas mixture. To measure total As (t-As) concentrations, AAS together with the hydride generation (HS 55 batch system) was used (Analytik Jena AG 2019). Ion chromatography (Metrohm, 883 Basic IC plus) was used to analyze ions. The concentration of cations was determined with a Metrosep C4-150/4.0 column according to DIN EN ISO 14911, and the concentrations of anions with a Metrosep A Supp 5-150/4.0 column. Total organic carbon (TOC) was analyzed with a Shimadzu TOC-L Analyzer. All measurements were repeated at least twice unless specified. Additionally, samples were analyzed by the certified commercial lab QUATEST3 in Ho Chi Minh City, Vietnam.

RESULTS AND DISCUSSION

Raw water quality at the pilot site

The chemical and physical properties of the raw groundwater in comparison to the Vietnamese standard for drinking water quality are summarized in Table 1. Analysis was carried out at different times before commissioning. In addition to initial elevated concentrations of Fe^{2+} ($c_{max} = 3.1$ mg/L) and t-As ($c_{max} = 11$ µg/L), the groundwater at the pilot site has an increased salinization with TDS concentrations of $c > 1.5$ g/L. In order to assess the groundwater quality at the beginning of the pilot trials, relevant water parameters were monitored over a period of 1 month directly before commissioning. During this period, an average of 15.5 m^3 of water was extracted on a daily basis, while no infiltration was carried out. This volume of water is greater than the extraction limit of 8.3 m^3/d. Measurements showed a slow increase in Fe^{2+} and t-As concentrations during this month of sampling until the start of the SAR operation, which indicates that the extraction of large amounts of groundwater without treatment has an influence on the concentrations given hydrogeologically. However, the averaged concentrations of Fe^{2+} and Mn^{2+} were similar compared with the values from March 2018, and the averaged t-As level decreased slightly, remaining below the WHO guideline value of $c = 10$ µg/L, which also indicates that the rise in the contaminant levels during the measurement period was within the naturally occurring fluctuations. The value for the t-As concentration from the pre-commissioning phase differed from the initial measured value of 11 µg/L (see Table 1) 1 year before and can also be attributed to naturally occurring fluctuations.

Iron, As and Mn removal (SAR)

Results for the first 181 days of operation of the SAR plant for t-As, Fe^{2+} and Mn^{2+} removal are shown in Figure 4.

Table 1 | Analysis of raw groundwater at the pilot site in Trà Vinh

Parameter	Unit	Sampling[a] 2 August 2017	Sampling[b] 2 August 2017	Sampling[a] 7 March 2018	Pre-commissioning[a,c]		Vietnamese standard[d]
Ph	–	7.2	NM	6.9	7.1	±0.3	6.5–8.5
EC	mS/cm	3.3	NM	3.3	3.3	±0.3	NA
t-As	µg/L	10	11	2.6	2.3	±1	10
Fe^{2+}	mg/L	1.7	3.1	1.8	1.8	±0.7	0.3
Mn^{2+}	mg/L	0.66	0.69	0.26	0.25	±0.05	0.3
F^-	mg/L	NM	NM	NM	0.92	±0.003	1.5
Cl^-	mg/L	886	827	955	1,035	±7	250
NO_3^-	mg/L	11	NM	NM	8.1	±5	50
SO_4^{2-}	mg/L	95.2	97.8	138	101	±1	250
PO_4^{3-}	mg/L	BDL	BDL	BDL	BDL	–	NA
Na^+	mg/L	343	338	374	379	±22	200
K^+	mg/L	12	12	10	13	±1	NA
Ca^{2+}	mg/L	170	178	NM	204	±21	120[e]
Mg^{2+}	mg/L	111	111	110	120	±8	NA
NH_4^+	mg/L	2.1	2.4	2.1	3.1	±0.3	3
HCO_3^-	mg/L	NM	437	NM	NM	–	NA
TOC	mg/L	16.2	NM	NM	4.2	±2	NA

[a]Analyzed in own laboratories (see the section Materials and methods).
[b]Certified commercial lab: QUATEST3, HCMC, Vietnam.
[c]Averaged value from samples taken before commissioning between 25 May 2018 and 28 June 2018 (number of samples = 8).
[d]QCVN 01 : 2009/BYT.
[e]Calculated from hardness limit $CaCO_3 = 300$ mg/L.
NM: Not measured; BDL: below detection limit; NA: not applicable.

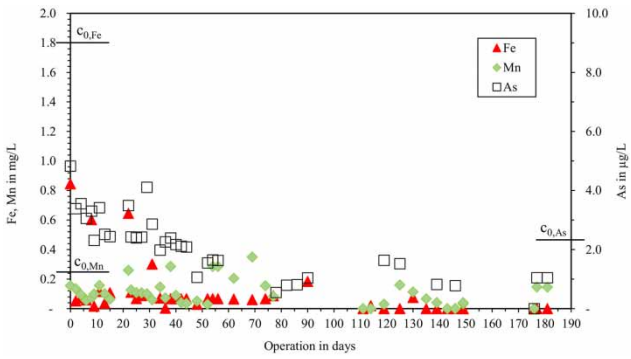

Figure 4 | Iron, As and manganese removal with SAR treatment at the pilot site in Trà Vinh.

The averaged background concentrations measured during 34 days before commissioning (see Table 1) are considered as the initial concentrations for Fe^{2+}, Mn^{2+} and t–As, which are indicated at the *y*-axes as $c_{0,Fe}$, $c_{0,Mn}$ and $c_{0,As}$, respectively. During this time, the t-As and Fe^{2+} concentrations increased to $c_{As} > 4.8$ µg/L and $c_{Fe} > 2.1$ mg/L due to natural fluctuations and the extraction of unusually high amounts of water without infiltration cycles. The Mn concentration remained at $c_{Mn} > 0.24$ mg/L. Thus, the t-As concentration at the first day of SAR operation is $c_{As} > c_{0,As}$, also indicating the slower removal of As over Fe. Measurements in Table 1 also show that the t-As concentrations can be above 10 µg/L on this site.

After the start of operation, the concentration of As was continuously lowered following the removal of Fe^{2+} until the value 0.55 µg/L was reached on day 78, corresponding to elimination rates of 76%. The highest increase in t–As measured from day 91 to 120 from 1.0 to 1.6 µg/L follows the rise in Fe due to the technical failure of the pump outlined above. The t–As mobilization decreases immediately when normal operation continues from day 120. The last

measured value of t-As indicated a concentration of 1.1 µg/L and thus a removal of 54%. These two abovementioned removal rates for t-As are acceptable for an already significantly low background concentration of $c_{0,As} = 2.3$ µg/L. In earlier SAR experiments in South Vietnam, Cañas Kurz *et al.* (2020) showed with the same technology for high background concentrations of $c_{As} = 80$ µg/L a removal to $c_{As} < 5$ µg/L.

After initiating the first infiltration cycle, results show an immediate strong decrease in Fe concentrations within the first days of operation. Values as low as $c = 0.1$ mg/L for Fe^{2+} were measured after day 3 until constant values were achieved after day 37. Manganese concentration dropped linearly to below $c = 0.06$ mg/L within the first 7 days of operation, indicating a removal of 75%. However, Fe concentrations spiked irregularly within the first 30 days and increases in Mn^{2+} were observed throughout the 70 days of operation. Subsequently, concentrations do not exceed the initial value of $c_{0,Mn}$. Increases in Fe^{2+} and Mn^{2+} concentrations can be explained by minor technical problems during pilot operation including the incomplete infiltration cycles caused by malfunction of the submersible pump, overextraction (abstraction above the plant capacity of 8.3 m^3), and the failure of the water meter. These technical complications did not stop the process completely but, by not maintaining a correct extraction/infiltration ratio, interrupted the proper operation of the infiltration and abstraction cycles temporarily, which causes the concentration peaks (Luong *et al.* 2019).

In general, the results show a slow but continuous removal for all three species (Fe^{2+}, As and Mn^{2+}), and after 181 days of operation, no breakthrough above the limits for drinking water standard was observed.

In addition, ammonium (NH_4^+) was lowered from initial concentrations of 3.1 mg/L to an average of 1.1 mg/L corresponding to a removal of 65%.

Desalination results (MCDI)

To determine the ideal operational parameters for the MCDI plant, laboratory tests with synthetic water (setup 2) have been carried out. Subsequently, these parameters were adjusted for the operation at the pilot site with setup 1. The comparison between lab and pilot scale is discussed below.

The optimum process parameters for the different MCDI setups employed are shown in Table 2. The general goal is to achieve a diluate concentration of <450 mg $_{NaCl}$/L or <600 mg $_{TDS}$/L (WHO guidelines for 'good' drinking water; WHO 2017). Different operational parameters are therefore chosen for the different setups, such as the electrical current for CC charge and the adsorption times in addition to the discharge current and discharge phase times, which are adapted accordingly. To obtain a reasonable water recovery rate, the discharge phase times have to be set as short as possible. Thus, the CC in the discharge phase is set always higher than the CC during the charge phase. The TDS concentrations of the feed are set depending on the quality of the groundwater ($EC = 3.3$ mS/cm, converted with the K factor, see the section Materials and methods) and are averaged over the time of the experiment ($t_{tot,av} = 64$ min) as well as the diluate salt concentration. Best results with setup 1 are obtained at a slightly lower feed $EC = 3.12$ mS/cm than the overall seasonal average at the pilot site. The test with setup 2 in the laboratory showed a lower $SEC_{CDI,2} = 0.97$ kWh/m^3 (see Equation

Table 2 | Characteristics of the two MCDI plant setups with optimal operation parameters

Setup number	Units	1	2
Feed EC	mS/cm	3.12	3.29
Feed TDS concentration	mg/L	1,560	1,645
Diluate TDS concentration	mg/L	188	410
TDS reduction	mg/L	1,372	1,235
Energy use in one cycle	kJ	4.7	10.2
Product rate	L/d	477	400
SEC of the desalination module	kWh/m^3	1.75	0.97
Charge efficiency	–	75%	77%
Water recovery	–	33%	65%
TDS removal	–	88%	75%
Constant current (charge phase)	A	50	12.3
Constant current (discharge phase)	A	66	54.1
Voltage limit	V	1.3	1.3
Water flow (charge phase)	L/min	1	0.4
Phase time (charge phase)	s	45	440
Cycle time	s	135	630

(1)). After the transition from the laboratory to the pilot site, a higher $SEC_{CDI,1} = 1.75$ kWh/m^3 has been achieved, treating a complex salt matrix with setup 1 and thus bivalent cations as well, which can reduce Na^+ and Cl^- ions adsorption (Suss 2017). The corresponding energy values were measured at the outlet of the power supply for the MCDI module, giving the values for the actual desalination performance, without considering the further periphery. The component within the home-made experimental setup with the highest energy consumption is the power supply, which has very poor energy efficiency as low as 20%, and is thus the component with the highest potential for improvement. This is achieved in large commercial modules by a design that allows a more efficient conversion of an alternate current (AC) grid with the voltage of 230 V in a low ampere range to a direct current circuit with a voltage of <2 V and a high ampere range. Therefore, the energy loss of the power supply in the experimental units (setup 1 and setup 2) is not considered in the following (see Equation (2)).

The $SEC_{CDI,sys}$ can be calculated using Equation (2) to $SEC_{CDI,sys,1} = 2.20$ kWh/m^3 for setup 1 and $SEC_{CDI,sys,2} = 1.08$ kWh/m^3 for setup 2. The performance of the diaphragm pump ($P_{p,1} = 8.9$ W and $P_{p,2} = 1.8$ W, respectively), which is proportional to the pressure loss over the MCDI module, is then added to the power consumption for the desalination. It should be noted that MCDI can also be operated by gravitational flow in combination with a flow regulating valve, and consequently, the diaphragm pump can be omitted. The comparatively low water recovery in setup 1 of 33% shows that the size of the module should be increased to handle the water under pilot conditions. Thus, a higher water recovery and hence a lower *SEC* value could be achieved.

The desalination with MCDI setup 1 on the pilot site with operational parameters of Table 2 started after the pre-treatment with SAR was running stably on day 112 (see Figure 4). The late application of MCDI also ensures that the Fe^{2+} concentration in groundwater is in compliance with the manufacturer's feed water recommendations of $Fe^{2+} < 0.5$ mg/L (Voltea 2016). Although the desalination efficiency of MCDI can be mainly accessed by the overall salt removal (see Table 2), the adsorption efficiency for selected ions was taken within 12 weeks to evaluate the overall ion removal especially for Fe^{2+} and t-As.

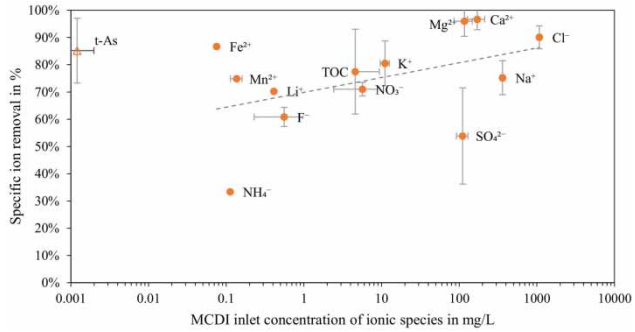

Figure 5 | MCDI averaged specific removal of ionic species and TOC at different initial concentrations. Values averaged from inlet and outlet concentrations. If more than one measurement, horizontal and vertical bars show the standard deviation of the averaged values. *X*-axis: log-scale. Dotted line: logarithmic trend excluding t-As.

Figure 5 shows the elimination rates for ionic species at their given averaged inlet concentrations at the MCDI module (after SAR treatment, Figure 4) in between days 112 and 181. The samples were taken from the inlet and the diluate stream of the MCDI. The electrosorption of the bivalent Fe^{2+} ions was very high, at 87%. The t–As concentration after the SAR treatment of averaged 1.2 µg/L was lowered to below 0.18 µg/L through MCDI, indicating another removal of 85%.

The results also showed specific ion removals of 75% Na^+, 90% Cl^-, and up to 97% for Ca^{2+} and Mg^{2+}, indicating a stronger selective adsorption of bivalent cations as shown in literature results (Suss 2017). However, lower sulfate (SO_4^{2-}) mitigation was observed with only 54% removal, which can be explained by the increasing hydrated radius and decreasing permeability of the bivalent ions Ca^{2+}, Mg^{2+} and SO_4^{2-}, respectively (Tansel *et al.* 2006; Li *et al.* 2016).

Renewable energy supply

Measurements of solar radiation at the pilot plant location and the results of the PV panels show an average daily production of 11.2 ± 1.3 kWh/d (the upper line in gray) for the measured days between May 2018 and December 2019 with an average radiation of 338 ± 53 W/m^2 (the lower line in blue) and maximum radiation values between 990 and 1215 W/m^2 (Figure 6). The average WT power production was 3.4 ± 0.3 kWh/d. The average wind speed measured at

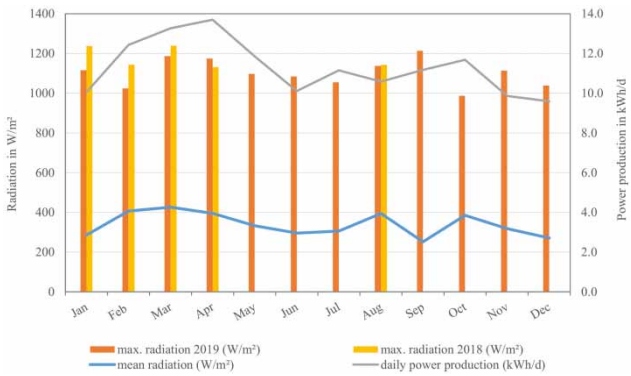

Figure 6 | Monthly solar radiation and solar energy supply at the pilot location averaged from measurements from May 2018 to December 2019.

the pilot location was 4.0 ± 1.3 m/s. However, the WT could not be operated continuously due to noise complaints from neighbors.

The power generation and power consumption at the pilot site for four different scenarios is shown in Figure 7(a)–7(d). Figure 7(a) shows the power production of the PV panels (blue line) on a typical clear-sky, sunny day with no power consumption and a peak performance of $P_{peak} = 2060$ W. The yellow line with the same absolute values as the power production shows the feeding to the grid (net-metering). Figure 7(b) shows the PV power production and the supply of the pilot plant. The purple line shows the load of the pilot plant at a typical daily operation including the desalination with MCDI (24 h operation) with averaged $P_{CDI,tot} = 176$ W for the MCDI module and its periphery, SAR (abstraction and oxygenation cycle with the SCALA 2 pump, beginning at 18:00) and the submersible pump for feeding T1 during SAR operation with averaged $P_{SAR} = 1{,}732$ W. In this example, the load is supplied by the grid during night time (yellow line: positive). When solar power production starts at sunrise (06:00), the load is supplied by PV. The addition of the power production (blue line, positive) and the load (purple line, negative) equals the amount of energy supplied by or fed into the grid (yellow line, positive or negative, respectively).

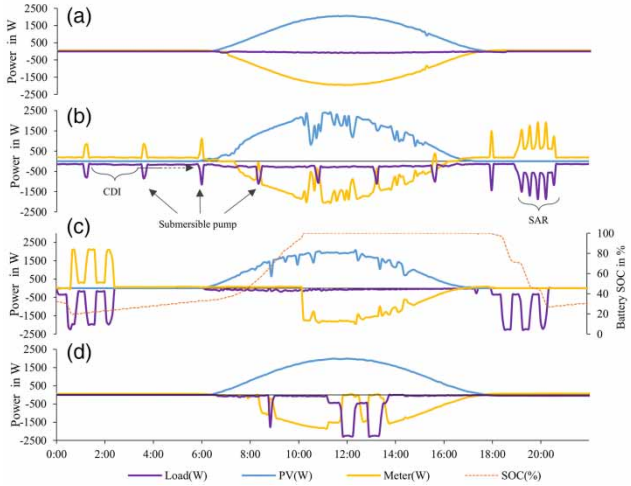

Figure 7 | Solar powered energy supply of the pilot plant for different scenarios: (a) solar power generation (PV, blue line) without consumption (purple line) and feed onto grid (yellow line); (b) typical daily course of load (purple) including MCDI (24 h), SAR (op. at 18:00) and submersible pump (intermittent peaks); (c) semi-autonomous supply using battery (orange line) and grid for SAR operation (two cycles at night 18:00 and 00:00, respectively); (d) close to autonomous supply with PV for SAR (one cycle, 11:30). (Please refer to the online version of this paper to see this figure in colour: doi:10.2166/wrd.2020.031).

Figure 7(c) shows the semi-autonomous supply for the SAR when using both battery (orange line) and grid for two infiltration cycles during the night at 18:00 and 00:00, respectively. Following the discharge of the battery (orange line) after the first SAR cycle (18:00), the second SAR cycle (00:00) is supplied directly from the grid (yellow line). Battery recharge for the next cycle is then powered by PV, and SOC is completed (SOC = 100%) around 10:15. After this, the energy produced is fed into the grid (net-metering: yellow line decreasing) following the absolute values of the power production (blue line). Figure 7(d) shows the autonomous supply with PV for SAR operation without MCDI (one cycle, 11:30).

To use the solar power production more efficiently, the operation of SAR is shifted during day time as shown in Figure 7(d), demonstrating that an autonomous (off-grid) operation is feasible. By doing this, the consumption of energy from the grid can be significantly reduced by 3.65 kWh, which is the average energy of one full infiltration cycle, and thus the degree of autonomy is increased. A high degree of autonomy or even of grid solutions is worthwhile, especially for a possible operation on the numerous small Vietnamese islands.

In total, the average energy consumption for the operation of the SAR and MCDI module was 11.6 kWh/d. A degree of autonomy for the overall pilot plant of 97% could be achieved with a total energy supply of 11.2 kWh with

Table 3 | Summary of all *SEC* values in kWh/m^3 to evaluate the pilot plant

SEC_{SAR}	$SEC_{SAR,supply}$	$SEC_{SAR,tot}$	SEC_{CDI}	$SEC_{CDI,sys}$	$SEC_{pilot,tot}$
0.88	0.89	1.77	1.75	2.20	3.97

Note: Energy values of the following processes were taken into account for *SEC* values with respective indices: *SAR*: SAR treatment; SAR,supply: water supply from subsurface to household; SAR,tot: *SAR* plus SAR.supply; CDI: desalination only and no periphery; CDI,sys: desalination plus pump for the CDI system; pilot,tot: SAR,tot plus CDI,sys.

PV. The energy deficit was supplied by the power grid. If the wind power of 3.4 ± 0.3 kWh/d at an average wind speed of 4.0 ± 1.3 m/s can be used, the degree of autonomy increases to 126% and thus 3.0 kWh/d of electrical energy can be fed into the grid, which provides governmental financial benefit (see the section State of the art), or used for a different purpose.

It should be noted that the *SEC* of the total SAR process consists of an *SEC* for the subsurface treatment (SEC_{SAR}) and an *SEC* for supply of the product water ($SEC_{SAR,supply}$) (see Table 3). On the pilot site, the water is supplied by the PENTAX well pump to the rooftop of the house via an elevation of $H = 14$ m, with an average performance of $P_{wp} = 1{,}332$ W and a maximum water flow of $\dot{V} = 1{,}500$ L/h. Hence, the *SEC* value for supply is $SEC_{SAR,supply} = 0.89$ kWh/m^3. This value is highly dependent on construction and environmental conditions. The advantage of supplying the water on the rooftop is that no additional auxiliary pumps are needed to maintain the necessary pressure to provide treated water to the complete household, which is standard in Vietnamese households due to nonconstant pressure conditions in the public water grid.

The SAR module treated 8.3 m^3 of water, which is potentially available subsurface. However, at the pilot site, on average 3.64 m^3 of water were supplied to the user. The MCDI module produced 0.48 m^3 of drinking water per day. Thus, the *SEC* values equal to $SEC_{SAR} = 0.88$ kWh/m^3 ($SEC_{SAR,supply} = 0.89$ kWh/m^3), $SEC_{CDI} = 1.75$ kWh/m^3 ($SEC_{CDI,sys} = 2.20$ kWh/m^3) and hence the overall $SEC_{pilot,tot} = 3.97$ kWh/m^3.

The two treatment stages produce water in different qualities and amounts, which can be used for different purposes modularly. The water produced from the SAR treatment can be used for washing, for example, and the diluate of the MCDI for drinking.

CONCLUSION AND OUTLOOK

- SAR has proved a feasible *in situ* remediation technique for Fe, Mn and As in brackish anoxic aquifers in combination with MCDI desalination, resulting in a total $SEC_{pilot,tot} = 3.97$ kWh/m^3 of drinking water. Fe, Mn and As concentrations could be lowered below drinking regulation standards. The TDS removal by the MCDI of 1,372 mg/L to a concentration of $c = 188$ mg/L could be achieved.
- Finally, two water streams were produced, which can be modularly adjusted according to the local requirements. One treated by SAR with low Fe, Mn and As but high TDS, for washing purposes and another additionally treated by MCDI, for drinking purposes.
- The very low efficiency of the power supply for the MCDI module shows the improvement potential of the homemade desalination plant on the pilot site.
- Based on the previous experience, it is expected that the efficiency of the system can be increased by upscaling the capacity of the MCDI module.
- The supply with 3 kW_p solar PV energy was feasible and a degree of autonomy of 97% for the water treatment was achieved, producing 0.48 m^3 drinking water and supplying 3.16 m^3 of washing water per day (out of the potential 8.3 m^3). Using a 2 kW_p WT, a degree of autonomy of 126% can be realized. However, the use of the WT was difficult because the high noise level was not accepted by those living in the neighborhood.

ACKNOWLEDGEMENTS

This project received funding from the German Ministry of Education and Research under the grant agreement no. 02WAV1413.

DATA AVAILABILITY STATEMENT

All relevant data are included in the paper or its Supplementary Information.

REFERENCES

AlMarzooqi, F. A., Al Ghaferi, A. A., Saadat, I. & Hilal, N. 2014 Application of capacitive deionisation in water desalination: a review. *Desalination* **342**, 3–15. https://doi.org/10.1016/j.desal.2014.02.031.

Analytik Jena AG 2019 Operating Manual novAA 800 AAS, 05.19.ed. Documentation number: 10-1430-002-23. https://www.analytik-jena.com/fileadmin/content/products/novAA/Manual_novAA_800_en_0519.pdf.

Annaduzzaman, M., Bhattacharya, P., Biswas, A., Hossain, M., Ahmed, K. M. & van Halem, D. 2018 Arsenic and manganese in shallow tubewells: validation of platform color as a screening tool in Bangladesh. *Groundwater Sustainable Dev.* **6**, 181–188. https://doi.org/10.1016/j.gsd.2017.11.008.

Ayers, J. C., Goodbred, S., George, G., Fry, D., Benneyworth, L., Hornberger, G., Roy, K., Karim, M. R. & Akter, F. 2016 Sources of salinity and arsenic in groundwater in southwest Bangladesh. *Geochem. Trans.* **17**, 1–22. https://doi.org/10.1186/s12932-016-0036-6.

Berg, M., Tran, H. C., Nguyen, T. C., Pham, H. V., Schertenleib, R. & Giger, W. 2001 Arsenic contamination of groundwater and drinking water in Vietnam: a human health threat. *Environ. Sci. Technol.* **35**, 2621–2626. https://doi.org/10.1021/es010027y.

Brecht, H., Dasgupta, S., Laplante, B., Murray, S. & Wheeler, D. 2012 Sea-level rise and storm surges. *J. Environ. Dev.* **21**, 120–138. https://doi.org/10.1177/1070496511433601.

Buschmann, J., Berg, M., Stengel, C., Winkel, L., Sampson, M. L., Trang, P. T. K. & Viet, P. H. 2008 Contamination of drinking water resources in the Mekong delta floodplains: arsenic and other trace metals pose serious health risks to population. *Environ. Int.* **34**, 756–764. https://doi.org/10.1016/j.envint.2007.12.025.

Cañas Kurz, E. E., Luong, V. T., Hellriegel, U., Leidinger, F., Luu, T. L., Bundschuh, J. & Hoinkis, J. 2020 Iron-based subsurface arsenic removal (SAR): results of a long-term pilot-scale test in Vietnam. *Water Res.* **181**, 115929. https://doi.org/10.1016/j.watres.2020.115929.

Colombani, N., Osti, A., Volta, G. & Mastrocicco, M. 2016 Impact of climate change on salinization of coastal water resources. *Water Resour. Manage.* **30**, 2483–2496. https://doi.org/10.1007/s11269-016-1292-z.

Ćurko, J., Mijatović, I., Matošić, M., Jakopović, H. K. & Bošnjak, M. U. 2011 As(V) removal from drinking water by coagulation and filtration through immersed membrane. *Desalination* **279**, 404–408. https://doi.org/10.1016/j.desal.2011.06.043.

Dasgupta, S., Akhter, F., Zahirul, K., Khan, Z., Choudhury, S. & Nishat, A. 2014a *River Salinity and Climate Change Evidence From Coastal Bangladesh (No. 6817)*.

Dasgupta, S., Hossain, M. M., Huq, M. & Wheeler, D. 2014b *Climate Change, Groundwater Salinization and Road Maintenance Costs in Coastal Bangladesh (No. 7147)*.

Datta, S., Johannesson, K., Mladenov, N., Sankar, M., Ford, S., Vega, M., Neal, A., Kibria, M., Krehel, A. & Hettiarachchi, G. 2014 Groundwater-sediment sorption mechanisms and role of organic matter in controlling arsenic release into aquifer sediments of Murshidabad area (Bengal basin), India: Proceedings of the 5th International Congress on Arsenic in the Environment. In: *One Century of the Discovery of Arsenicosis in Latin America (1914–2014) As 2014*, pp. 95–97. https://doi.org/10.1201/b16767-37

Do, T. N., Burke, P. J., Baldwin, K. G. H. & Nguyen, C. T. 2020 Underlying drivers and barriers for solar photovoltaics diffusion: the case of Vietnam. *Energy Policy* **144**, 111561. https://doi.org/10.1016/j.enpol.2020.111561.

Elcik, H., Cakmakci, M., Sahinkaya, E. & Ozkaya, B. 2013 Arsenic removal from drinking water using low pressure membranes. *Ind. Eng. Chem. Res.* **52**, 9958–9964. https://doi.org/10.1021/ie401393p.

Figoli, A., Hoinkis, J. & Bundschuh, J. (Eds.) 2016 *Membrane Technologies for Water Treatment: Removal of Toxic Trace Elements with Emphasis on Arsenic, Fluoride and Uranium, Sustainable Water Developments*. CRC Press.

Figoli, A., Fuoco, I., Apollaro, C., Chabane, M., Mancuso, R., Gabriele, B., De Rosa, R., Vespasiano, G., Barca, D. & Criscuoli, A. 2020 Arsenic-contaminated groundwaters remediation by nanofiltration. *Sep. Purif. Technol.* **238**. https://doi.org/10.1016/j.seppur.2019.116461

Fritz, M., Hohmann, C. & Tettenborn, F. 2020 Framework conditions to design sustainable business models for decentralised water treatment technologies in Viet Nam for international technology providers. *J. Water Reuse Desalin* **10** (4), 317–331. https://doi.org/10.2166/wrd.2020.016.

Hien, L. T., Quy, P. N. & Viet, N. T. 2009 *Assessment of Salinity Intrusion in the Red River Under Effect of Climate Change*. ICEC.

Hossain, M., Williams, P. N., Mestrot, A., Norton, G. J., Deacon, C. M. & Meharg, A. A. 2012 Spatial heterogeneity and kinetic regulation of arsenic dynamics in mangrove sediments: The Sundarbans, Bangladesh. *Environ. Sci. Technol.* **46**, 8645–8652. https://doi.org/10.1021/es301328r.

Kundu, D. K., Gupta, A., Mol, A. P. J., Rahman, M. M. & van Halem, D. 2018 Experimenting with a novel technology for provision of safe drinking water in rural Bangladesh: the case of sub-surface arsenic removal (SAR). *Technol. Soc.* **53**, 161–172. https://doi.org/10.1016/j.techsoc.2018.01.010.

Le Luu, T. 2019 Remarks on the current quality of groundwater in Vietnam. *Environ. Sci. Pollut. Res.* https://doi.org/10.1007/s11356-017-9631-z

Li, Y., Zhang, C., Jiang, Y., Wang, T. J. & Wang, H. 2016 Effects of the hydration ratio on the electrosorption selectivity of ions during capacitive deionization. *Desalination* **399**, 171–177. https://doi.org/10.1016/j.desal.2016.09.011.

Luong, V. T., Cañas Kurz, E. E., Hellriegel, U., Luu, T. L., Hoinkis, J. & Bundschuh, J. 2018 Iron-based subsurface arsenic removal technologies by aeration: a review of the current

state and future prospects. *Water Res.* **133**, 110–122. https://doi.org/10.1016/j.watres.2018.01.007.

Luong, V. T., Cañas Kurz, E. E., Hellriegel, U., Luu, T. L., Hoinkis, J. & Bundschuh, J. 2019 Iron-based subsurface arsenic removal by aeration (SAR) – results of a pilot-scale plant in Vietnam. In: *Environmental Arsenic in A Changing World As 2018* (J. Bundschuh & P. Bhattacharya, eds). CRC Press/Balkema, London, UK, pp. 418–419.

Ngo-Duc, T. 2014 Climate change in the coastal regions of Vietnam. In: *Coastal Disasters and Climate Change in Vietnam*. Elsevier, pp. 175–198. https://doi.org/10.1016/B978-0-12-800007-6.00008-3

Nickson, R. T., Mcarthur, J. M., Ravenscroft, P., Burgess, W. G. & Ahmed, K. M. 2000 Mechanism of arsenic release to groundwater, Bangladesh and West Bengal. *Appl. Geochem.* **15**, 403–413. https://doi.org/10.1016/S0883-2927(99)00086-4.

Rahman, M. M., Bakker, M., Freitas, S. C. B., van Halem, D., van Breukelen, B. M., Ahmed, K. M. & Badruzzaman, A. B. M. 2014 Exploratory experiments to determine the effect of alternative operations on the efficiency of subsurface arsenic removal in rural Bangladesh. *Hydrogeol. J.* **23**, 19–34. https://doi.org/10.1007/s10040-014-1179-0.

Rahman, M. M. M., Bakker, M., Patty, C. H. L. H. L., Hassan, Z., Röling, W. F. M. F. M., Ahmed, K. M. M. & van Breukelen, B. M. M. 2015 Reactive transport modeling of subsurface arsenic removal systems in rural Bangladesh. *Sci. Total Environ., Arsenic Environ.* **537**, 277–293. https://doi.org/10.1016/j.scitotenv.2015.07.140.

Rott, U. & Friedle, M. 2000 25 jahre unterirdische Wasseraufbereitung in Deutschland. *Wasser Spec.* **141**, 99–107.

Sankar, M. S., Vega, M. A., Defoe, P. P., Kibria, M. G., Ford, S., Telfeyan, K., Neal, A., Mohajerin, T. J., Hettiarachchi, G. M., Barua, S., Hobson, C., Johannesson, K. & Datta, S. 2014 Elevated arsenic and manganese in groundwaters of Murshidabad, West Bengal, India. *Sci. Total Environ.* **488–489**, 570–579. https://doi.org/10.1016/J.SCITOTENV.2014.02.077.

Sarkar, A. R. & Rahman, O. T. 2001 *In-situ Removal of Arsenic – Experiences of DPHE-Danida Pilot Project*. Available from: http://archive.unu.edu/env/Arsenic/Sarkar.pdf (accessed 14 January 2020).

Schmidt, S.-A., Gukelberger, E., Hermann, M., Fiedler, F., Großmann, B., Hoinkis, J., Ghosh, A., Chatterjee, D. & Bundschuh, J. 2016 Pilot study on arsenic removal from groundwater using a small-scale reverse osmosis system towards sustainable drinking water production. *J. Hazard. Mater.* **318**, 671–678. https://doi.org/10.1016/j.jhazmat.2016.06.005.

Sen Gupta, B. 2008 *Subterranean Arsenic Removal Technology for In Situ Groundwater Arsenic and Iron Treatment [WWW Document]*.

Shih, M.-C. 2005 An overview of arsenic removal by pressure-driven membrane processes. *Desalination* **172**, 85–97. https://doi.org/10.1016/j.desal.2004.07.031.

Smedley, P. L., Nicolli, H. B., Macdonald, D. M. J., Barros, A. J. & Tullio, J. O. 2002 Hydrogeochemistry of arsenic and other inorganic constituents in groundwaters from La Pampa, Argentina. *Appl. Geochem.* **17**, 259–284. https://doi.org/10.1016/S0883-2927(01)00082-8.

Stopelli, E., Duyen, V. T., Mai, T. T., Trang, P. T. K., Viet, P. H., Lightfoot, A., Kipfer, R., Schneider, M., Eiche, E., Kontny, A., Neumann, T., Glodowska, M., Patzner, M., Kappler, A., Kleindienst, S., Rathi, B., Cirpka, O., Bostick, B., Prommer, H., Winkel, L. H. E. & Berg, M. 2020 Spatial and temporal evolution of groundwater arsenic contamination in the Red River delta, Vietnam: interplay of mobilisation and retardation processes. *Sci. Total Environ.* **717**, 137143. https://doi.org/10.1016/j.scitotenv.2020.137143.

Suss, M. E. 2017 Size-based ion selectivity of micropore electric double layers in capacitive deionization electrodes. *J. Electrochem. Soc.* **164**, E270–E275. https://doi.org/10.1149/2.1201709jes.

Tan, C., He, C., Tang, W., Kovalsky, P., Fletcher, J. & Waite, T. D. 2018 Integration of photovoltaic energy supply with membrane capacitive deionization (MCDI) for salt removal from brackish waters. *Water Res.* **147**, 276–286. https://doi.org/10.1016/j.watres.2018.09.056.

Tansel, B., Sager, J., Rector, T., Garland, J., Strayer, R. F., Levine, L., Roberts, M., Hummerick, M. & Bauer, J. 2006 Significance of hydrated radius and hydration shells on ionic permeability during nanofiltration in dead end and cross flow modes. *Sep. Purif. Technol.* **51**, 40–47. https://doi.org/10.1016/j.seppur.2005.12.020.

van Halem, D. 2011 *Subsurface Iron and Arsenic Removal for Drinking Water Treatment in Bangladesh*. Water Management Academic Press.

van Halem, D., Heijman, S. G. J., Amy, G. L. & van Dijk, J. C. 2009 Subsurface arsenic removal for small-scale application in developing countries. *Desalination* **248**, 241–248. https://doi.org/10.1016/j.desal.2008.05.061.

Voltea 2016 *Technical Bulletin: Feedwater Guidelines*. Sassenheim. Available from: https://voltea.com/wp-content/uploads/2016/03/402D021_Rev02-Technical-Bulletin_Water-Quality-Criteria.pdf (accessed 08 August 2020).

Vu, D. T., Yamada, T. & Ishidaira, H. 2018 Assessing the impact of sea level rise due to climate change on seawater intrusion in Mekong Delta, Vietnam. *Water Sci. Technol.* **77**, 1632–1639. https://doi.org/10.2166/wst.2018.038.

WaKap 2016 *WaKap – Ein Projekt zur Wasseraufbereitung mittels Kapazitiver Deionisierung [WWW Document]*. Available from: www.wakap.de (accessed 30 August 2019).

Walton, N. R. G. 1989 Electrical conductivity and total dissolved solids – what is their precise relationship? *Desalination* **72**, 275–292. https://doi.org/10.1016/0011-9164(89)80012-8.

Wang, Y., Le Pape, P., Morin, G., Asta, M. P., King, G., Bártová, B., Suvorova, E., Frutschi, M., Ikogou, M., Pham, V. H. C., Vo, P. L., Herman, F., Charlet, L. & Bernier-Latmani, R. 2018 Arsenic speciation in Mekong delta sediments

depends on their depositional environment. *Environ. Sci. Technol.* **52**, 3431–3439. https://doi.org/10.1021/acs.est.7b05177.

Wang, L., Dykstra, J. E. & Lin, S. 2019 Energy efficiency of capacitive deionization. *Environ. Sci. Technol.* **53**, 3366–3378. https://doi.org/10.1021/acs.est.8b04858.

Wassmann, R., Hien, N. X., Hoanh, C. T. & Tuong, T. P. 2004 Sea level rise affecting the Vietnamese Mekong Delta: water elevation in the flood season and implications for rice production. *Clim. Change* **66**, 89–107. https://doi.org/10.1023/B:CLIM.0000043144.69736.b7.

Wheeler, D. 2011 *Quantifying Vulnerability to Climate Change: Implications for Adaptation Assistance (No. 240)*. Washington, DC.

WHO 2017 *Guidelines for Drinking-Water Quality: Fourth Edition Incorporating the First Addendum*, 4th edn. World Health Organization, Geneva, Switzerland.

Winkel, L. H. E., Trang, P. T. K., Lan, V. M., Stengel, C., Amini, M., Ha, N. T., Viet, P. H. & Berg, M. 2011 Arsenic pollution of groundwater in Vietnam exacerbated by deep aquifer exploitation for more than a century. *Proc. Natl. Acad. Sci.* **108**, 1246–1251. https://doi.org/10.1073/pnas.1011915108.

Zhao, Y., Wang, Y., Wang, R., Wu, Y., Xu, S. & Wang, J. 2013 Performance comparison and energy consumption analysis of capacitive deionization and membrane capacitive deionization processes. *Desalination* **324**, 127–133. https://doi.org/10.1016/j.desal.2013.06.009.

First received 3 April 2020; accepted in revised form 2 September 2020. Available online 5 October 2020